A&A 631, A42 (2019)
https://doi.org/10.1051/0004-6361/201935337

Astronomy & Astrophysics

Relativistic electron impact ionization cross sections of carbon ions and application to an optically thin plasma

Miguel A. de Avillez[1,2], Mauro Guerra[3], José Paulo Santos[3], and Dieter Breitschwerdt[2]

[1] Department of Mathematics, University of Évora, R. Romão Ramalho 59, 7000 Évora, Portugal
e-mail: mavillez@galaxy.lca.uevora.pt
[2] Zentrum für Astronomie und Astrophysik, Technische Universität Berlin, Hardenbergstrasse 36, 10623 Berlin, Germany
[3] Laboratory of Instrumentation, Biomedical Engineering and Radiation Physics (LIBPhys-UNL), Department of Physics, Faculty of Sciences and Technology, New University of Lisbon, 2829-516 Caparica, Portugal

Received 22 February 2019 / Accepted 8 September 2019

ABSTRACT

Context. Ionization through electron impact is a fundamental process associated with the evolution of the ionic structure and emissivity of astrophysical plasmas. Over several decades substantial efforts have been made to measure and calculate the ionization cross sections of ionization through electron impact of different ions shell by shell, in particular, of carbon ions. Spectral emission codes use electron-impact ionization cross sections and/or rates taken from different experimental and theoretical sources. The theoretical cross sections are determined numerically and include a diversity of quantum mechanical methods. The electron-impact ionization database therefore is not uniform in the methods, which makes it hard to determine the reason for the deviations with regard to experimental data. In many cases only total ionization rates for Maxwell–Boltzmann plasmas are available, which makes calculating inner-shell ionization in collisional-radiative models using thermal and nonthermal electron distribution functions difficult. A solution of this problem is the capability of generating the cross sections with an analytical method using the minimum number of atomic parameters. In this way, uniformity in the database is guaranteed, and thus deviations from experiments are easily identified and traced to the root of the method.
Aims. The modified relativistic binary encounter Bethe (MRBEB) method is such a simple analytical scheme based on one atomic parameter that allows determining electron-impact ionization cross sections. This work aims the determination of K- and L-shell cross sections of the carbon atom and ions using the MRBEB method and show their quality by: (i) comparing them with those obtained with the general ionization processes in the presence of electrons and radiation (GIPPER) code and the flexible atomic code (FAC), and (ii) determining their effects on the ionic structure and cooling of an optically thin plasma.
Methods. The MRBEB method was used to calculate the inner-shells cross sections, while the plasma calculations were carried out with the collisional+photo ionization plasma emission software (CPIPES). The mathematical methods used in this work comprise a modified version of the double-exponential over a semi-finite interval method for numerical integrations, Gauss-elimination method with scaled partial pivoting for the solution of systems of linear equations, and an iterative least-squares method to determine the fits of ionization cross sections.
Results. The three sets of cross sections show deviations among each other in different energy regions. The largest deviations occur near and in the peak maximum. Ion fractions and plasma emissivities of an optically thin plasma that evolves under collisional ionization equilibrium, derived using each set of cross sections, show deviations that decrease with increase in temperature and ionization degree. In spite of these differences, the calculations using the three sets of cross sections agree overall.
Conclusions. A simple model like the MRBEB is capable of providing cross sections similar to those calculated with more sophisticated quantum mechanical methods in the GIPPER and FAC codes.

Key words. atomic data – atomic processes – radiation mechanisms: thermal – plasmas

1. Introduction

Carbon is the fourth most abundant element in nature after H, He, and O. It has a solar abundance of log[C/H] = −3.57 (Asplund et al. 2009) and thus contributes much to the emissivity of a plasma. Jointly with He, carbon contributes to the second peak maximum observed in the radiative cooling function of a plasma that evolves under collisional ionization equilibrium (see, e.g., Shapiro & Moore 1976; Boehringer & Hensler 1989; Schmutzler & Tscharnuter 1993; Sutherland & Dopita 1993; Gnat & Sternberg 2007; de Avillez et al. 2010). In addition, CI and CII ions (through fine-structure and metastable transitions) are the main contributors to radiative cooling at temperatures below 10^3 K. The other contributors are OI, SiI, SiII, SI, FeI, and FeII through fine-structure lines and OI, OII, SiI, SiII, SiI, SII, FeI, and FeII through metastable transitions (see, e.g., Dalgarno & McCray 1972; Wolfire et al. 1995, 2003). Furthermore, carbon plays an important role in the chemistry of molecular clouds (see, e.g., Larson 1981; Pavlovski et al. 2002; Glover 2007) as well as in shocks (see, e.g., Hollenbach & McKee 1989).

The cross sections of the electron-impact ionization of carbon ions have been extensively studied by means of theoretical calculations and experimental measurements. Since the seminal work of Bethe (1930), who derived the correct form of the cross section at high electron energies, much effort has been invested to calculate the cross sections using empirical and semi-empirical methods or more sophisticated quantum mechanical numerical calculations. Compilations comprising theoretical and experimental ionization cross sections for the carbon atom and

ions, including the best fits to these, that have been popular in the Atomic Physics and Astrophysics communities, were published over the years by Lotz (1967, 1968), Bell et al. (1983; hereafter BL83), Arnaud & Rothenflug (1985, AR85), Lennon et al. (1988, L88), Suno & Kato (2006, SK06), Mattioli et al. (2007, M07), Dere (2007, D2007), to name only a few.

The recommended total (BL83; L88; SK06, and M07) and partial (AR85) cross sections are parametrized using the Younger (1981) formula:

$$\sigma(E) = \frac{10^{-13}}{I_{Z,z}^2 u}\left[\sum_{i=1}^{n_{\max}} A_i \left(1-\frac{1}{u}\right)^i + B\ln(u) + C\frac{\log u}{u}\right] \mathrm{cm}^2, \quad (1)$$

where $u = E/I_{Z,z}$, $I_{Z,z}$ is the ionization potential (in eV) of the ion with atomic number Z and ionic state z, E is the incident electron kinetic energy (in eV); $n_{\max} = 2$ in Younger (1981) and AR85 and 5 in BL83, SK06 and M07. The coefficient B (the Bethe constant) is determined from the photoionization cross section, $\sigma_{\rm ph}$, through

$$B = 4I_{Z,z}\int_{I_{Z,z}}^{\infty}\frac{1}{\epsilon}\frac{\mathrm{d}f}{\mathrm{d}\epsilon}\mathrm{d}\epsilon = \frac{I_{Z,z}}{\pi\alpha}\int_{I_{Z,z}}^{\infty}\frac{\sigma_{\rm ph}}{\epsilon}\mathrm{d}\epsilon, \quad (2)$$

where $\mathrm{d}f/\mathrm{d}\epsilon$ is the optical differential oscillator strength. At high energies, the cross section tends to the Bethe limit (see, e.g., Younger 1981; Pradhan & Nahar 2011),

$$\lim_{u\to\infty}\sigma(E) = \frac{1}{u}B\ln(u). \quad (3)$$

When B is known, the coefficients A_i and C are determined directly from a least-squares fitting procedure. Hence, the fit to the cross section has the correct asymptote at high energies. In AR85, the ionization potential $I_{Z,z}$ and the coefficients A_i, B, and C refer to the subshell j of the initial ion. The total direct ionization cross section is then obtained by summing over all the subshells.

Bell et al. (1983) and Lennon et al. (1988) adopted the experimental data of Brook et al. (1978) for CI and extrapolated the data beyond 1 keV using a fitting equation to the Born approximation. The recommended curve for the CII ionization cross section follows the cross-beam measurements of Aitken et al. (1971) and at high energies the Coulomb-Born calculations of Moores (1972). For CIII and CIV ionization, Bell and collaborators adopted the Coulomb-Born calculations of Jakubowicz & Moores (1981). In the case of CIII ionization, a small contribution from inner-shell ionization was included. The cross section for ionization of CV was obtained by scaling the ionization cross section of BIV along the isosequence. For CVI the calculations by Younger (1980) have been adopted.

Arnaud & Rothenflug (1985) considered the ionization cross sections of the different subshells. The CVI cross-section (shell 1s) parameters were determined from the distorted wave-exchange approximation calculations of Younger (1981). For CV (shell $1s^2$) a fit to the measured cross section available at the Electron-Impact Ionization Data of Multicharged Ions database (EIIDMI; Crandall et al. 1979a)[1] was carried out. The theoretical values of Younger (1981) for the direct ionization from shell $1s^2$ of the Li-like ion CIV were adopted, while for the 2s shell ionization, the Crandall et al. (1979b) data were kept. Excitation-autoiozation contributions to the CIV ion were taken into account; the derived formulae are presented in Appendix A of AR85. For CIII (shells $1s^2$ and $2s^2$), AR85 adopted the calculations by Younger (1981) along the sequence. The fitting parameters for the CII and CI ionization of shell $2s^2$ were deduced by extrapolation from higher-z elements. The fit to the CII 2p shell ionization cross section is based on the measurements of Aitken et al. (1971), and those of CI were derived from the measurements by Brook et al. (1978). The parameter B was derived from the photoionization cross section of Reilman & Manson (1979).

Suno & Kato (2006) adopted for CVI and CV the cross sections calculated using the distorted-wave method with exchange (Pattard & Rost 1999) and the distorted-wave Born method (Fang et al. 1995), respectively. For CIV, the experimental data of Knopp et al. (2001) were selected. Because of excitation-autoionization, the cross section has two peaks. For CIII, the experimental data of Woodruff et al. (1978) were chosen, and for CII and CI, the experimental data of Yamada et al. (1989) and Brook et al. (1978) were used, respectively.

Mattioli et al. (2007) adopted cross sections from theoretical and experimental data: the CVI and CV cross sections were taken from Arnaud & Rothenflug (1985). For CIV, the Crandall et al. (1979b) data were complemented with those available at the EIIDMI database. For CIII, the data of Falk et al. (1983) for low metastable contributions and that of Loch et al. (2005) were adopted. Similarly to SK06, the cross sections of CII and CI were taken from Yamada et al. (1989) and Brook et al. (1978), respectively.

The Dere (2007) compilation combines experimental cross sections with those obtained with the flexible atomic code (FAC)[2] (Gu 2002, 2008). For CVI, D2007 favored the parametric fit of Fontes et al. (1999) to their relativistic distorted -wave approximation cross-section calculations for ionization from the 1s shell; the CV cross section is determined with the FAC. For CIV and CIII, direct ionization and excitation-autoionization cross sections calculated with the FAC were adopted; for CIII, the 1s and 2s subshells were taken into account for the direct ionization cross sections, while for EA the $1s2l^3$ and $1s2l^23l'$ transitions were considered. The Yamada et al. (1989) and Brook et al. (1978) cross-section measurements were adopted for CII and CI, respectively. The total cross sections, available in version 8.0.7 of the CHIANTI atomic database[3] (Del Zanna et al. 2015), are provided as spline nodes for a scaled energy U and cross section $\Sigma_{Z,z}$ given by

$$U = 1 - \frac{\log f}{\log(u-1+f)} \quad (4)$$

and

$$\Sigma_{Z,z} = \frac{u\sigma_{Z,z}I_{Z,z}}{\log(u)+1}, \quad (5)$$

respectively. In these expressions $f = 2$ is an adjustable parameter, $\sigma_{Z,z}$ is the unscaled cross section, and u, and $I_{Z,z}$ have the meanings related in previous paragraphs.

Further calculations using sophisticated quantum mechanical methods have been carried out in the last two decades by Bote et al. (2009), Abdel-Naby et al. (2013), and Wang et al. (2013) for CI, Ludlow et al. (2008), Ballance et al. (2011), Pindzola et al. (2012), and Lecointre et al. (2013) for CII, Fogle et al. (2008) for CIII, Pindzola et al. (2012) for CIV, and Fontes et al. (1999) for CVI. Some of these authors also reported

[1] http://www-cfadc.phy.ornl.gov

[2] http://www-amdis.iaea.org/FAC

[3] http://www.chiantidatabase.org

experimental measurements that were used to compare with the theoretical cross sections, for instance, Wang et al. (2013) for CI, Lecointre et al. (2013) for CII, and Fogle et al. (2008) for CIII.

Empirical classical and semiclassical analytical methods have also been adopted over the years to calculate ionization cross sections of different ions. These include the binary-encounter-Bethe (BEB; Kim & Rudd 1994) model[4] and its derivatives, for example, the relativistic BEB (Kim et al. 2000) and the modified relativistic BEB (Guerra et al. 2012, MRBEB) models. The advantage of these models is their simple analytical expressions and the small number of adopted parameters that depend on the binding energy, on the energy of the impacting electron, and on the shielding by inner electrons, for instance. The MRBEB model has been applied to calculate the K-, L- and M-shell ionization cross sections of several atoms, with Z varying between 6 and 83 (Guerra et al. 2012), and for several ionization stages of Ar, Fe, and Kr (Guerra et al. 2013), and U (Guerra et al. 2015). The model provides reliable direct ionization cross sections, and the relative differences to experimental data are smaller than 10% for the inner shells of neutral atoms and 20% for highly charged ions (Guerra et al. 2012, 2013). For a review of these models, see Llovet et al. (2014), for example.

We here use the MRBEB method to calculate the K- and L-shell cross sections of the carbon ions and convolve them with the Maxwell–Boltzmann electron distribution function in order to obtain the corresponding ionization rates. A further application is made to the evolution of an optically thin plasma in order to obtain the radiative losses due to electron-impact ionization, bremsstrahlung, and line emission. The structure of this paper is as follows. Section 2 describes the MRBEB model and the calculation of the K- and L-shell ionization cross sections of the carbon atom and ions. Section 3 describes the use of the calculated cross sections in determining the ionization structure and radiative losses of an optically thin plasma that evolves under collisional ionization equilibrium. Section 4 closes the paper with a discussion and final remarks.

2. Modified relativistic binary encounter Bethe model cross sections

2.1. The MRBEB model

The MRBEB model uses an analytical approach containing a single atomic parameter (the binding energy of the electron to be ionized) and takes into account the energy of the impacting electron and the shielding of the nuclear charge by the bound electrons of the target ion. Therefore, the number of electrons in the inner shells up to the subshell that is ionized acts as a screening of the nuclear potential as seen by the primary electron. In contrast to the MRBEB, the other binary encounter Bethe and relativistic binary encounter Bethe models require two input parameters (the binding energy and the kinetic energy of the bound electron).

The MRBEB cross section, denoted by $\sigma_{nlj,\mathrm{LS}}$, refers to the ionization of an *nlj* electron in an atom or ion in a given initial state LS. The cross section takes into account the relativistic interactions between the incident and target electrons during inner-shell ionization of heavy atoms or ions. The determination of the cross section requires knowledge of one single parameter: the binding energy of the target electron. The cross section

[4] BEB combines the Mott cross section with the high-incident energy behavior of the Bethe cross section.

Table 1. Binding energies (eV) calculated with the MDFGME code for the ground-state configurations of CI–CVI.

Ion	Config.	Shells			
		1s	2s	$2p_{1/2}$	$2p_{3/2}$
C^{0}	$1s^2 2s^2 2p^2$	308.24671	19.21208	11.78503	11.79174
C^{1+}	$1s^2 2s^2 2p^1$	323.82728	31.40751	24.61858	
C^{2+}	$1s^2 2s^2$	344.30589	46.11313		
C^{3+}	$1s^2 2s^1$	366.88819	64.37863		
C^{4+}	$1s^2$	391.39542			
C^{5+}	$1s^1$	490.01853			

is given by (Guerra et al. 2012)

$$\sigma_{nlj,\mathrm{LS}} = \frac{4\pi a_o^2 \alpha^4 N}{\left(\beta_t^2 + \chi\beta_b^2\right) 2b'} \left[A(\beta_t, t, b') + B(t, t', b')\right] \ \mathrm{cm}^2 \tag{6}$$

with

$$A(\beta_t, t, b') = 0.5\left[\ln\left(\frac{\beta_t^2}{1-\beta_t^2}\right) - \beta_t^2 - \ln(2b')\right]\left(1 - \frac{1}{t^2}\right) \tag{7}$$

and

$$B(t, t', b') = 1 - \frac{1}{t} - \frac{\ln t}{1+t}\frac{1+2t'}{(1+t'/2)^2} + \frac{b'^2}{(1+t'/2)^2}\frac{t-1}{2} \tag{8}$$

with

$$t = \frac{E}{B},\ \beta_t^2 = 1 - \frac{1}{(1+t')^2},\ b' = \frac{B}{m_e c^2},$$
$$t' = \frac{E}{m_e c^2},\ \beta_b^2 = 1 - \frac{1}{(1+b')^2}.$$

In these equations, E denotes the kinetic energy of the impacting electron, B is the binding energy of the target electron, and c stands for the speed of light, while m_e is the electron mass; a_o and α are the Bohr radius and the fine-structure constant, respectively. The scaling $\frac{1}{\beta^2 + \chi\beta_b^2}$ includes the effects of the shielding of the nucleus by the target-bound electron through the parameter χ , which is therefore related to the shielding coefficient $C_{nlj}(Z)$ and the binding energy B of the target electron through the relation $\chi = 2\,\mathrm{Ry}\, C_{nlj}(Z)/B$ (Ry is the Rydberg energy). The shielding of the nucleus is described by

$$C_{nlj}(Z) = 0.3\frac{Z_{eff,nlj}^2}{2n^2} + 0.7\frac{Z_{\mathrm{eff},n'l'j'}^2}{2n'^2}, \tag{9}$$

where $n'l'j'$ stands for the next subshell after subshell nlj, ordered in energy, and Z_{eff} is the screening effect (Guerra et al. 2017).

2.2. Cross-section calculations

Using the MRBEB model, we calculated the K- and L-shell ionization cross sections for carbon and its ions. The binding energies of each target electron were calculated using the multi-configuration Dirac-Fock (MCDF) theoretical framework with the multi configuration Dirac-Fock and general matrix element (MCDFGME) code (Indelicato & Desclaux 1990), which evaluates level energies, including correlation and first- and second-order quantum electrodynamics corrections. Table 1 displays

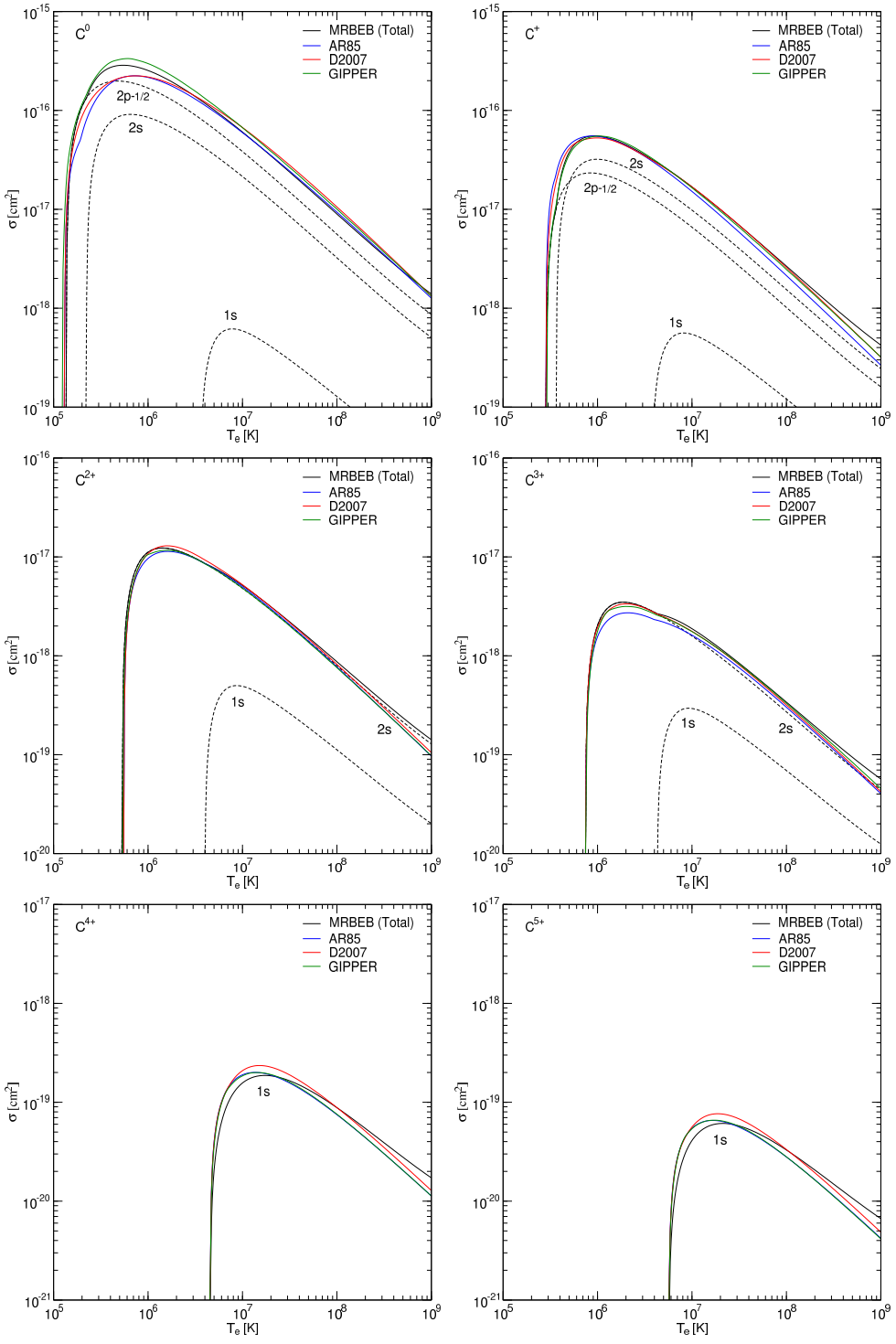

Fig. 1. K- and L-shell (dashed black lines) and total (solid black lines) ionization cross sections of the carbon atom and ions calculated with the MRBEB model and total cross sections in AR85 (blue lines) and D2007 (red lines) calculated with the GIPPER code (green lines).

the binding energies obtained with the MCDF method without electronic correlation beyond the intermediate coupling using the Rodrigues et al. (2004) ground-state configurations for the different ions. First-order retardation terms of the Breit operator and the Uelhing contribution to the vacuum polarization terms were included self-consistently. The Wichmann-Kroll and Kallen-Sabry contributions, as well as higher-order Breit retardation terms and other QED effects, such as self-energy, were included as perturbations.

Figure 1 displays the inner shell (dashed black lines) and total (solid black lines) cross sections of the carbon ions calculated with the MRBEB model. In addition, the figure also shows the total cross sections of Arnaud & Rothenflug (1985, blue lines), Dere (2007, red lines), and those calculated with the GIPPER code[5] (Fontes et al. 2015, green lines). In general, the total MRBEB, GIPPER, and D2007 cross sections have a similar distribution for CII, CIII, and CIV ions. Small deviations occur during the approach to the peak maximum (CII), in the peak maximum (CIII ans CIV), and after the peak maximum (CIII and CIV). The total MRBEB cross sections for CII–CVI ions

[5] GIPPER provides electron-impact ionization, photoionization, and autoionization data using the distorted-wave approach.

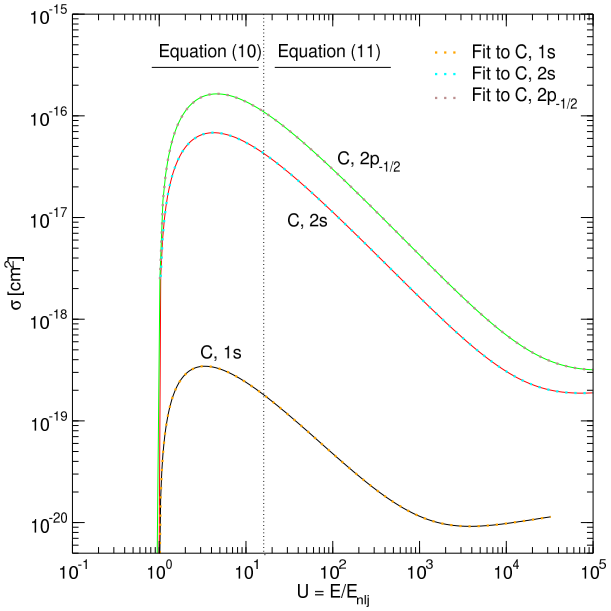

Fig. 2. Fit (dotted lines) to the electron-impact ionization cross sections (solid lines) of CI using Eqs. (10) and (11).

dominate the others for $T > 10^8$ K because of the relativistic effects, which are taken into account in the calculations.

The MRBEB and GIPPER cross sections have small deviations for CI, CII, CIII, and CIV near and at the peak maximum. The largest deviations between the MRBEB and GIPPER cross sections occur for CV and CVI ions starting at the approach to the peak maximum. The GIPPER cross sections overlap those discussed in AR85. The cross sections in D2007 have the highest values for CV and CVI ions at peak maximum and at high energies up to 10^8 K when the MRBEB cross section takes over. Clearly, a simple analytical method depending on a single atomic parameter gives similar results to those provided by the more sophisticated GIPPER and FAC methods.

2.3. Fits to the cross sections

The MRBEB cross sections were fit (for CI see Fig. 2) with the functional (Bote et al. 2009)

$$\sigma(E) = 4\pi a_o^2 \frac{U-1}{U^2}\left(a_1 + a_2 U + \frac{a_3}{1+U} + \frac{a_4}{(1+U)^3} + \frac{a_5}{(1+U)^5}\right)^2 \quad (10)$$

for $U = E/E_{nlj} \leq 16$, while for higher energies a variation of their Eq. (5) was used,

$$\sigma(E) = \frac{U}{U+1.513}\frac{4\pi a_o^2}{\beta^2}\left[b_1\chi + b_2\frac{\chi}{P} + b_3 + b_4\left(1-\beta^2\right)^{1/4} + b_5\frac{1}{P}\right], \quad (11)$$

with $\chi = 2\ln P - \beta^2$, and where $\beta = v/c = \sqrt{E(E+2m_ec^2)}/(E+m_ec^2)$ and $P = p/(m_ec) = \sqrt{E(E+2m_ec^2)}/m_ec^2$ are the velocity and momentum of the impacting electron, respectively, a_0 is the Bohr radius and the parameters a_1–a_5 and b_1–b_5 (displayed in Tables 2 and 3) are characteristic of each element and electron shell. These parameters were calculated using a least-squares fit. The two right columns in the tables represent the maximum relative differences below and above 0, respectively. The absolute relative difference is the largest of the absolute of these two maxima. The relative difference is given by

$$\Delta\sigma = \left(1.0 - \frac{\sigma_{\rm fit}}{\sigma}\right)100\%. \quad (12)$$

The maximum relative differences above and below zero are labeled $\Delta\sigma^-$ and $\Delta\sigma^+$, respectively. The maximum absolute relative differences occur for $U = E/E_{nlj} \leq 16$, that is, with the fitting of Eq. (10). The maximum error is found to be 1.315% and occurs for the cross section associated with shell $2p_{1/2}$ of CI. This is followed for absolute relative differences of 0.915% and 0.81% for the fit of the EII cross sections of the 2s shell of CI and CIII. For the fits associated with energies of $U = E/E_{nlj} > 16$, the maximum absolute relative difference is lower than 0.07%.

3. Application to an optically thin plasma

We discussed different sets of cross sections for the ionization of the carbon atom and ions and now compare their effects on the ionization structure and on the cooling of an optically thin plasma characterized by a Maxwell–Boltzmann (MB) electron distribution function. The determination of the ionic state of the plasma as well as its emissivity is important for theoretical models as well as observations of absorption features in the diffuse medium where Li-like ions (CIV, NV, and OVI) are important to distinguish between different ionization mechanisms, such as turbulent mixing layers (Slavin et al. 1993), shock ionization (Dopita & Sutherland 1996), conduction interfaces (Borkowski et al. 1990), and radiative cooling (Edgar & Chevalier 1986). These processes in turn are used to study high-velocity clouds (see, e.g., Indebetouw & Shull 2004) or gas in the Local Bubble (de Avillez & Breitschwerdt 2009). In addition, the emission caused by CV and CVI is important to understand the spectra associated with the processes described above, as well as with that of ionizing (Masai 1984) or recombining (de Avillez & Breitschwerdt 2012) plasmas or in the soft X-ray spectra that are observed in supernova remnants. Spectral fitting codes for X-ray emitting space plasmas are often used to determine the temperature and ionization state of a plasma. Orbiting X-ray observatories such as *Chandra* and *XMM-Newton* have chip-based X-ray detectors that can barely resolve individual lines for diffuse low surface brightness plasmas like the hot interstellar medium. Therefore it is important to quantify as well as possible the contribution of various ions such as carbon to the total spectrum.

For each set of cross sections we followed the evolution of a gas parcel cooling under collisional ionization equilibrium conditions from an initial temperature of 10^9 K where it is completely ionized. The plasma was composed of hydrogen and carbon with solar abundances (Asplund et al. 2009) and a hydrogen particle density, $n_{\rm H}$, of 1 cm^{-3}. These calculations are referred to as the MRBEB, GIPPER, and D2007 models.

The processes we took into account are electron-impact ionization, radiative recombination including cascades into the ground state, dielectronic recombination, bremsstrahlung, and line emission. No charge-exchange reactions were considered. Hence, and because the evolution is in collisional ionization equilibrium, the ionization structure of each element (composed of atoms and ions) can be treated independently of the other elements. Thus, the evolution of the carbon atom and ions is the same whether the plasma is composed only of carbon or of any set of elements including carbon.

Table 2. a_1–a_5 fit coefficients for Eq. (10).

Z	Ion	Shell	E_{nlj} (eV)	a_1	a_2	a_3	a_4	a_5	$\Delta\sigma^-$ [%]	$\Delta\sigma^+$ [%]
6	0	1s	308.25	9.2135E−2	5.2082E−4	−1.1545E−1	1.1282E−1	−4.2654E−1	−0.262	0.157
6	0	2s	19.21	1.4319E+0	9.4133E−3	−2.3794E+0	3.1997E+0	−7.4347E+0	−0.446	0.915
6	0	$2p_{1/2}$	11.79	2.2848E+0	1.6892E−2	−4.1305E+0	6.4108E+0	−1.3503E+1	−0.691	1.315
6	1	1s	323.83	8.7667E−2	4.9960E−4	−1.0947E−1	1.0643E−1	−4.0545E−1	−0.257	0.152
6	1	2s	31.41	8.8915E−1	5.2590E−3	−1.3856E+0	1.6595E+0	−4.2079E+0	−0.341	0.400
6	1	$2p_{1/2}$	24.62	7.9808E−1	4.8760E−3	−1.2868E+0	1.6485E+0	−3.9822E+0	−0.370	0.598
6	2	1s	344.31	8.2511E−2	4.6848E−4	−1.0285E−1	1.0100E−1	−3.8499E−1	−0.264	0.156
6	2	2s	46.11	6.0642E−1	3.5623E−3	−9.4876E−1	1.1577E+0	−2.9084E+0	−0.326	0.808
6	3	1s	366.89	7.7408E−2	4.4358E−4	−9.6027E−2	9.4031E−2	−3.6139E−1	−0.257	0.151
6	3	2s	64.38	3.0939E−1	1.7414E−3	−4.6251E−1	5.3552E−1	−1.4540E+0	−0.266	0.372
6	4	1s	392.40	7.1514E−2	4.4140E−4	−1.0432E−1	1.1348E−1	−3.2384E−1	−0.302	0.375
6	5	1s	490.02	4.0675E−2	2.4722E−4	−5.8541E−2	6.5142E−2	−1.9087E−1	−0.271	0.404

Table 3. b_1–b_5 fit coefficients for Eq. (11).

Z	Ion	Shell	E_{nlj} (eV)	b_1	b_2	b_3	b_4	b_5	$\Delta\sigma^-$ [%]	$\Delta\sigma^+$ [%]
6	0	1s	308.25	2.3413E−06	1.8611E−08	2.0518E−05	−1.0142E−07	1.0674E−08	−0.037	0.013
6	0	2s	19.21	3.7588E−05	1.5327E−07	4.3387E−04	−1.3627E−06	3.3438E−07	−0.029	0.031
6	0	$2p_{1/2}$	11.79	6.1268E−05	2.3858E−07	7.3742E−04	−2.3593E−06	5.7687E−07	−0.049	0.070
6	1	1s	323.83	2.2285E−06	1.8076E−08	1.9421E−05	−9.8649E−08	9.8808E−09	−0.037	0.013
6	1	2s	31.41	2.2992E−05	1.0264E−07	2.5401E−04	−8.0300E−07	1.9680E−07	−0.030	0.028
6	1	$2p_{1/2}$	24.62	1.4666E−05	6.2439E−08	1.6563E−04	−5.2069E−07	1.2779E−07	−0.028	0.029
6	2	1s	344.31	2.0958E−06	1.7286E−08	1.8137E−05	−9.3739E−08	8.5368E−09	−0.035	0.014
6	2	2s	46.11	1.5661E−05	8.7277E−08	1.6699E−04	−5.6993E−07	1.4656E−07	−0.014	0.020
6	3	1s	366.89	1.9666E−06	1.6578E−08	1.6896E−05	−9.0602E−08	7.6196E−09	−0.034	0.015
6	3	2s	64.38	5.6097E−06	3.2241E−08	5.7912E−05	−1.8881E−07	4.7588E−08	−0.052	0.013
6	4	1s	392.40	1.8395E−06	2.7825E−08	1.5640E−05	−6.9840E−08	5.8958E−09	−0.008	0.007
6	5	1s	490.02	7.3612E−07	1.1832E−08	6.0987E−06	−3.1513E−08	1.0332E−09	−0.008	0.008

3.1. Thermal model

The ionization structure and emission properties of the gas parcel were followed using the thermal model described in de Avillez et al. (2018; for further details, see de Avillez in prep.). We therefore present a summary of this model in this subsection.

The density $n_{Z,z}$ (cm^{-3}) of an ion with atomic number Z and charge state z ($z = 0, \ldots, Z$) is determined from the populations of the neighboring charge states $z-1$, z, and $z+1$ through recombination ($\alpha_{Z,z}$, which includes radiative and dielectronic recombination) and collisional ionization ($S_{Z,z}$) rates from state z to $z-1$ and $z+1$, respectively. Hence, $n_{Z,z}$ is given by the system of equations

$$S_{Z,z-1} n_{Z,z-1} n_e - (S_{Z,z} + \alpha_{Z,z}) n_{Z,z} n_e + \alpha_{Z,z+1} n_{Z,z+1} n_e = 0, \quad (13)$$

where n_e is the electron density (cm^{-3}), which is obtained from

$$n_e = \sum_{z=1}^{Z} z\, n_{Z,z}. \quad (14)$$

By multiplying both sides of Eq. (13) by $1/n_Z$ (n_Z is the number density (cm^{-3}) of the species of atomic number Z) and factorizing n_e, the system of equations simplifies to

$$S_{Z,z-1} x_{Z,z-1} - (S_{Z,z} + \alpha_{Z,z}) x_{Z,z} + \alpha_{Z,z+1} x_{Z,z+1} = 0, \quad (15)$$

where $x_{Z,z} = n_{Z,z}/n_Z$ is the ion fraction (which varies between 0 and 1). This system of equations may be cast into the matrix form

$$AX = 0, \quad (16)$$

where X is a vector comprising all ion fractions $x_{Z,z}$ and A is a tridiagonal matrix with elements $S_{Z,z-1}$, $-(S_{Z,z} + \alpha_{Z,z})$, and $\alpha_{Z,z+1}$ at each row populating the diagonal band. The solution of this system of equations is straightforward using any Gauss-elimination method with or without pivoting. The final solution is then transformed into the ion density through

$$n_{Z,z} = x_{Z,z}\, n_Z = x_{Z,z}\, A(Z) n_H, \quad (17)$$

where $A(Z) = n_Z/n_H$ is the abundance of the species and n_H is the hydrogen number density (cm^{-3}).

The ionization rates, $S_{Z,z}$, are determined by convolving $\sigma(E)v$ with the MB electron distribution function,

$$f(E)\mathrm{d}E = \frac{2E^{1/2}}{\pi^{1/2}(k_B T)^{3/2}} e^{-E/k_B T}\mathrm{d}E, \quad (18)$$

and are given by

$$\langle \sigma v \rangle = \left(\frac{2}{m_e}\right)^{1/2} \int_{\Phi_{Z,z}}^{+\infty} \sigma(E) E^{1/2} f(E)\mathrm{d}E \quad \mathrm{cm}^3\mathrm{s}^{-1}, \quad (19)$$

where m_e is the electron mass (g), $\Phi_{z,z}$ is the ionization threshold (eV), and $\sigma(E)$ is the electron-impact ionization cross section (cm^2).

Radiative and dielectronic recombination rates used in these calculations are based on calculations with the AUTOSTRUCTURE code[6] (Badnell 2011) and are taken from Badnell (2006a) for HII and CII through CVII recombining to HI and CI through CVI, respectively. The radiative recombination rates have the functional

$$\alpha_{Z,z}^{\rm RR} = A\left[\left(\frac{T}{T_0}\right)^{1/2}\left(1+\left(\frac{T}{T_0}\right)^{1/2}\right)^{1-b}\left(1+\left(\frac{T}{T_1}\right)^{1/2}\right)^{1+b}\right]^{-1}, \quad (20)$$

where A (cm^3 s^{-1}), $T_{0,1}$ (K), and b (dimensionless) are fit coefficients. The latter is replaced by $b + C\exp(T_2/T)$ (C is dimensionless and T_2 is given in K) for low-ionization stages. The dielectronic recombination rates are given by the Burgess (1965) general formula

$$\alpha_{\rm DR}^{\rm MB} = \frac{1}{(k_{\rm B}T)^{3/2}}\sum_j c_j e^{-E_j/(k_{\rm B}T)} \quad {\rm cm^3 s^{-1}}, \quad (21)$$

whose coefficients are taken from Badnell (2006b) for HII and CVI, Bautista & Badnell (2007) for CV, Colgan et al. (2004, 2003) for CIV and CIII, respectively, and Altun et al. (2004) for CII.

The cooling due to electron-impact ionization ($\Lambda_{Z,z}^{\rm EII}$), bremsstrahlung ($\Lambda_{Z,z}^{\rm FF}$), and line (permitted, forbidden, and semi-forbidden) emission ($\Lambda_{Z,z}^{\rm LE}$) shown in Fig. 4 are given by

$$\Lambda_{Z,z}^{\rm EII} = n_{\rm e}n_{\rm H}A(Z)x_{Z,z}S_{Z,z}\Phi_{Z,z} \quad {\rm erg\ cm^{-3}\ s^{-1}}, \quad (22)$$

with $S_{Z,z}$ denoting the ionization rate (cm^3 s^{-1}) and $\Phi_{Z,z}$ is the ionization threshold (erg) of the ionizing ion,

$$\Lambda_{Z,z}^{\rm FF} = C\,z^2 n_{\rm e}n_{\rm H}A(Z)x_{Z,z}T^{1/2}\langle g_{\rm ff}(\gamma^2)\rangle \quad {\rm erg\ cm^{-3}\ s^{-1}}, \quad (23)$$

where $C = 1.4256\times10^{-27}$ erg cm^3 s^{-1} K$^{-1/2}$, T is the temperature (K), $\gamma^2 = z^2{\rm Ry}/k_{\rm B}T$ (Ry is the Rydberg energy) is the normalized temperature, and $\langle g_{\rm ff}(\gamma^2)\rangle$ is the total free-free Gaunt factor (see the details of its calculation in, e.g., de Avillez & Breitschwerdt 2015), and

$$\Lambda_{Z,z}^{\rm LE} = n_{\rm e}n_{\rm H}A(Z)x_{Z,z}\sum_{i,j,i<j} n_{Z,z,j}A_{ji}E_{ij} \quad {\rm erg\ cm^{-3}\ s^{-1}}, \quad (24)$$

where $n_{Z,z,j}$ is the population density of level j of the ion, A_{ji} is the spontaneous decay rate from level j to level i ($i < j$), and E_{ij} is the excitation energy between the two levels.

The level populations were calculated as described in de Avillez et al. (2018) by assuming that there is an equilibrium between excitation by electron impact and de-excitation by electron impact and spontaneous decay. Hence, the population of level j is obtained from the equation

$$\sum_{m<j} C_{mj}^{\rm e}n_{\rm e}n_{Z,z,m} + \sum_{n>j}\left(A_{nj}+C_{nj}^{\rm d}n_{\rm e}\right)n_{Z,z,n} - n_{Z,z,j}\left[\sum_{j<n}C_{jn}^{\rm e}n_{\rm e} + \sum_{j>m}\left(A_{jm}+C_{jm}^{\rm d}n_{\rm e}\right)\right] = 0, \quad (25)$$

coupled to the equation of mass conservation

$$\sum_j n_{Z,z,j} = n_{Z,z}. \quad (26)$$

[6] amdpp.phys.strath.ac.uk/tamoc/DATA/

In these equations $C_{mj}^{\rm e}$ and $C_{jn}^{\rm e}$ denote the excitation rates (cm^3 s^{-1}) from levels m to j ($m < j$) and j to n ($j < n$), respectively, while $C_{nj}^{\rm d}$ and $C_{jm}^{\rm d}$ denote the de-excitation rates (cm^3 s^{-1}) from levels n to j and j to m, respectively; A_{nj} and A_{jm} are the Einstein spontaneous decay coefficients (s^{-1}) from levels n to j and j to m, respectively; and $n_{Z,z,m}$ and $n_{Z,z,n}$ are the population densities (cm^{-3}) of levels m and n, respectively. The excitation and de-excitation rates are given by

$$C_{ij}^{\rm e} = 8.629\times10^{-6}\,T^{-1/2}\,\omega_i^{-1}\,e^{-y}\,\Upsilon_{ij}(T) \quad (27)$$

and

$$C_{ji}^{\rm d} = 8.629\times10^{-6}\,T^{-1/2}\,\omega_j^{-1}\,\mathcal{J}_{ji}(T), \quad (28)$$

where $y = E_{ij}/k_{\rm B}T$, $U = E_{\rm e}/E_{ij}$ is the reduced electron energy ($E_{\rm e}$ is the energy of the impacting electron), ω_i and ω_j are the statistical weights of levels i and j, respectively, and T is the temperature (K). The forms of the effective collision strength, $\Upsilon_{ij}(T)$, and of $\mathcal{J}_{ji}(T)$ relate to the collision strengths and are given by

$$\Upsilon_{ij}(T) = ye^y\int_1^{+\infty}\Omega_{ij}(U)\,e^{-yU}dU \quad (29)$$

$$\mathcal{J}_{ji}(T) = y\int_0^{+\infty}\Omega_{ji}(U')\,e^{-yU'}dU'. \quad (30)$$

The wavelengths, coefficients of spontaneous transitions, and the effective collision strengths were taken from version 8.0.7 of the CHIANTI atomic database[3].

3.2. Calculations and methods

The evolution of a gas parcel is calculated as follows: (i) at each temperature calculate first the ionization and recombination rates and solve the system of equations (15) to obtain the ion fractions, (ii) determine the ions and the electron densities from Eqs. (17) and (14), respectively, and (iii) obtain the emissivity due to the different processes using Eqs. (22)–(24).

The numerical methods used in these calculations are the same as in de Avillez et al. (2018), that is, (i) numerical integrations in semi-finite intervals, such as the ionization rates, were calculated with a precision of 10^{-15} using the double-exponential transformation method of Takahasi & Mori (1974), Mori & Sugihara (2001), and (ii) the system of equations (15) is solved using a Gauss-elimination method with scaled partial pivoting (Cheney & Kincaid 2008) and a tolerance of 10^{-15}.

3.3. Results

The carbon-ion fraction variations with temperature calculated with the MRBEB, GIPPER, and D2007 ionization cross sections are displayed in Fig. 3. Although there are some differences between the location of the ion profiles, the ionic structure shows similar properties in the three models: the same profiles for all the ions that are characterized with the dominance of CVII above 10^6 K, the dominance of CI below 10^4 K, and the classic CV plateau resulting from the K-shell ionization potential. The differences between the three models are reflected in the small deviation to the right for the MRBEB model with regard to the others, while the GIPPER model shows profiles that in some cases are to the left of the D2007 profiles and in other cases to the right, but always to the left of the MRBEB profiles. The reason

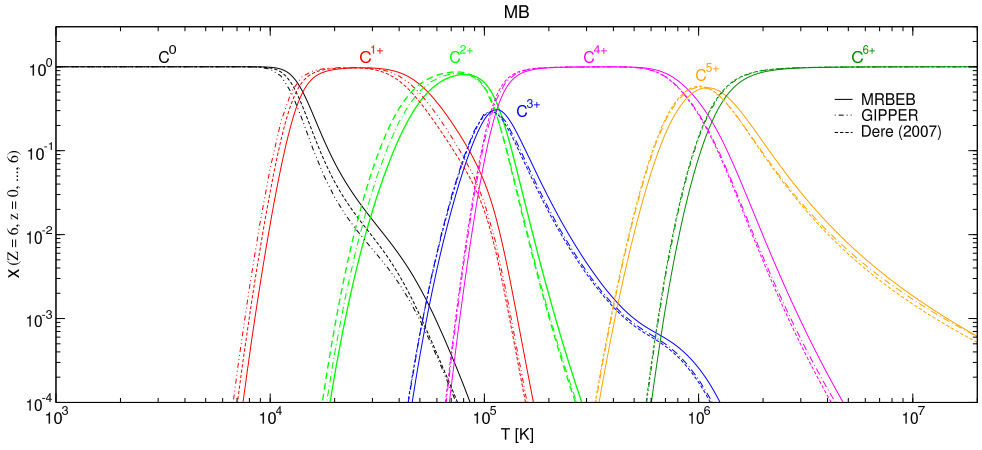

Fig. 3. Carbon ionic fraction variation with temperature evolving under collisional ionization equilibrium calculated with the MRBEB, GIPPER, and D2007 cross sections.

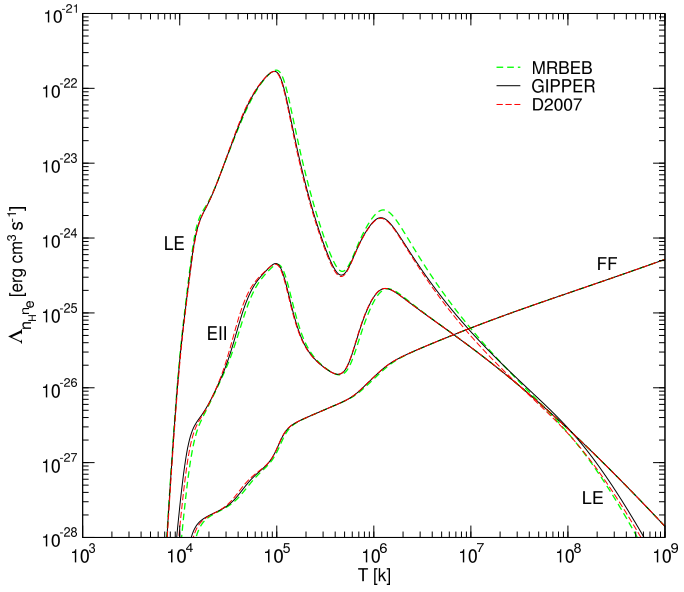

Fig. 4. Comparison of the cooling (erg cm3 s^{-1}), normalized to $n_e n_H$, due to electron-impact ionization (EII), bremsstrahlung (FF), and line emission (LE)) in a gas parcel evolving under collisional ionization equilibrium and calculated with MRBEB, GIPPER, and D2007 electron-impact ionization cross sections.

is that the threshold ionization energies in the MRBEB model are higher than those of the GIPPER and D2007 models, which leads to a delayed ionization of the carbon ions in comparison to the other cases.

Figure 4 displays the cooling (erg cm^3 s^{-1}), normalized to $n_e n_H$, due to electron-impact ionization (EII), bremsstrahlung (FF) using the total Gaunt factors calculated in de Avillez & Breitschwerdt (2017), for instance, and line (allowed, forbidden, and semi-forbidden) emission (LE) calculated with the three models (MRBEB, GIPPER, and D2007). Emissivities associated with different processes in different ranges in temperature overlap. For instance, above 10^5 K, the bremsstrahlung in the three models overlaps, except around 10^6. A complete overlap is visible above 2×10^6 K in electron-impact ionization and bremsstrahlung. In the latter the overlap extends to 10^5 K, except around 10^6 K. Deviations among the three models are seen in electron-impact ionization below 10^6 K and in line emission above 10^5 K, where the second peak maximum noticeably increases. For lower temperatures the line emission seems to be the same for all the models. The excess in emissivity in the MRBEB model is similar to that seen in the ionization structure (i.e., the deviation to the right). Although there are deviations in the models, they predict in general the same behavior and profile for the emissivities due to the different processes.

4. Discussion and final remarks

We applied the modified relativistic binary encounter Bethe model to calculate the K- and L-shell ionization cross sections of the carbon atom and ions and compare their variation with energy of the impacting electron with those calculated using the GIPPER code and those published by Dere (2007), which includes cross sections calculated with the flexible atomic code and the relativistic distorted wave approximation of Fontes et al. (1999), and experimental data.

In general, the three sets of cross sections have a similar profile for CII, CIII, and CIV ions, and small deviations occur during the approach to the peak (CII), in the peak (CIII and CIV), and after the peak (CIII and CIV) maximum. The total MRBEB cross sections for CII–CVI ions dominate the others for $T > 10^8$ K because of the relativistic effects. The MRBEB and GIPPER cross sections have small deviations for CI, CII, CIII, and CIV near and at the peak maximum, while the largest deviations occur in the approach to the peak maximum for CV and CVI. The D2007 cross sections have the highest values for CV and CVI ions at peak maximum and at high energies up to 10^8 K when the MRBEB cross sections take over. Although the FAC and GIPPER code use the distorted-wave method for the electron-impact ionization, the D2007 and GIPPER cross sections still show differences that can stem from the different numerical methods and the adopted atomic model.

We further explored the effects of the three sets of cross sections on the ion fractions of the carbon ions and on the cooling due to electron-impact ionization, bremsstrahlung, and line emission by an optically thin plasma that evolves under collisional ionization equilibrium and cooling from a temperature of 10^9 K. The three calculations, using the MRBEB, GIPPER, and D2007 cross sections, show deviations in the ion fractions of the same ion that decrease with increase in ionization degree: the strongest deviations occur in the lowest ionization states (CI–CIII), and the smallest deviations in the highest ionization states. These differences in the ion fractions propagate to the emissivities. At high temperatures the emissivities are similar in the three calculations, while in other temperature regimes noticeable differences are observed, for instance, in the second peak

maximum of the line emission around 10^6 K. The agreement between the emissivities calculated with the three sets of cross sections is nevertheless good overall.

The results show that a simple analytical model that only depends on one atomic parameter (the electron binding energy) is capable of providing electron-impact ionization cross sections similar to those calculated with the more sophisticated quantum mechanical methods in GIPPER and FAC. This shows that it is possible to build a database of cross sections associated with the atoms and ions of the ten most abundant elements in nature with the MRBEB method that can be used by any spectral emission code.

Acknowledgements. This research was supported by the projects "Enabling Green E-science for the SKA Research Infrastructure (ENGAGE SKA)" (M. A.; reference POCI-01-0145-FEDER-022217, funded by COMPETE 2020 and FCT) and "Ultra-high-accuracy X-ray spectroscopy of transition metal oxides and rare earths" (M. G.; reference PTDC/FIS-AQM/31969/2017, and SFRH/BPD/92455/2013 funded by FCT), and by the project UID/FIS/04559/2013 (LIBPhys). Partial support for M. A. and D. B. was provided by the Deutsche Forschungsgemeinschaft, DFG project ISM-SPP 1573. The calculations were carried out at the ISM – Xeon Phi cluster of the Computational Astrophysics Group, University of Évora, acquired under project "Hybrid computing using accelerators & coprocessors – modelling nature with a novell approach" (M. A.), InAlentejo program, CCDRA, Portugal.

References

Abdel-Naby, S. A., Ballance, C. P., Lee, T. G., Loch, S. D., & Pindzola, M. S. 2013, Phys. Rev. A, 87, 022708
Aitken, K. L., Harrison, M. F. A., & Rundel, R. D. 1971, J. Phys. B At. Mol. Phys., 4, 1189
Altun, Z., Yumak, A., Badnell, N. R., Colgan, J., & Pindzola, M. S. 2004, A&A, 420, 775
Arnaud, M., & Rothenflug, R. 1985, A&AS, 60, 425
Asplund, M., Grevesse, N., Sauval, A. J., & Scott, P. 2009, ARA&A, 47, 481
Badnell, N. R. 2006a, ApJS, 167, 334
Badnell, N. R. 2006b, A&A, 447, 389
Badnell, N. R. 2011, Comput. Phys. Commun., 182, 1528
Ballance, C. P., Loch, S. D., Ludlow, J. A., Abdel-Naby, S. A., & Pindzola, M. S. 2011, Phys. Rev. A, 84, 062713
Bautista, M. A., & Badnell, N. R. 2007, A&A, 466, 755
Bell, K. L., Gilbody, H. B., Hughes, J. G., Kingston, A. E., & Smith, F. J. 1983, J. Phys. Chem. Ref. Data, 12, 891
Bethe, H. 1930, Ann. Phys., 397, 325
Boehringer, H., & Hensler, G. 1989, A&A, 215, 147
Borkowski, K. J., Balbus, S. A., & Fristrom, C. C. 1990, ApJ, 355, 501
Bote, D., Salvat, F., Jablonski, A., & Powell, C. J. 2009, At. Data Nucl. Data Tables, 95, 871
Brook, E., Harrison, M. F. A., & Smith, A. C. H. 1978, J. Phys. B At. Mol. Phys., 11, 3115
Burgess, A. 1965, ApJ, 141, 1588
Cheney, W., & Kincaid, D. 2008, Numerical Mathematics and Computing, 6th edn. (Belmont: Thomson Brooks/Cole)
Colgan, J., Pindzola, M. S., Whiteford, A. D., & Badnell, N. R. 2003, A&A, 412, 597
Colgan, J., Pindzola, M. S., & Badnell, N. R. 2004, A&A, 417, 1183
Crandall, D. H., Gregory, D. C., & Phaneuf, R. A. 1979a, Electron Impact Ionization of Multicharged Ions, Tech. rep.
Crandall, D. H., Phaneuf, R. A., Hasselquist, B. E., & Gregory, D. C. 1979b, J. Phys. B At. Mol. Phys., 12, L249
Dalgarno, A., & McCray, R. A. 1972, ARA&A, 10, 375
de Avillez, M. A., & Breitschwerdt, D. 2009, ApJ, 697, L158
de Avillez, M. A., & Breitschwerdt, D. 2010, in The Dynamic Interstellar Medium: A Celebration of the Canadian Galactic Plane Survey, eds. R. Kothes, T. L. Landecker, & A. G. Willis, ASP Conf. Ser., 438, 313
de Avillez, M. A., & Breitschwerdt, D. 2012, ApJ, 756, L3
de Avillez, M. A., & Breitschwerdt, D. 2015, A&A, 580, A124
de Avillez, M. A., & Breitschwerdt, D. 2017, ApJS, 232, 12
de Avillez, M. A., Anela, G. J., & Breitschwerdt, D. 2018, A&A, 616, A58
Del Zanna, G., Dere, K. P., Young, P. R., Landi, E., & Mason, H. E. 2015, A&A, 582, A56
Dere, K. P. 2007, A&A, 466, 771
Dopita, M. A., & Sutherland, R. S. 1996, ApJS, 102, 161
Edgar, R. J., & Chevalier, R. A. 1986, ApJ, 310, L27
Fang, D., Hu, W., Chen, C., et al. 1995, At. Data Nucl. Data Tables, 61, 91
Falk, R. A., Stefani, G., Camilloni, R., et al. 1983, Phys. Rev. A, 28, 91
Fogle, M., Bahati, E. M., Bannister, M. E., et al. 2008, ApJS, 175, 543
Fontes, C. J., Sampson, D. H., & Zhang, H. L. 1999, Phys. Rev. A, 59, 1329
Fontes, C. J., Zhang, H. L., Abdallah, Jr., J., et al. 2015, J. Phys. B At. Mol. Phys., 48, 144014
Glover, S. C. O. 2007, MNRAS, 379, 1352
Gnat, O., & Sternberg, A. 2007, ApJS, 168, 213
Gu, M. 2002, in APS Meeting Abstracts, B17.075
Gu, M. F. 2008, Can. J. Phys., 86, 675
Guerra, M., Parente, F., Indelicato, P., & Santos, J. P. 2012, Int. J. Mass Spectrom., 313, 1
Guerra, M., Parente, F., & Santos, J. P. 2013, Int. J. Mass Spectrom., 348, 1
Guerra, M., Stöhlker, T., Amaro, P., Machado, J., & Santos, J. P. 2015, J. Phys. B At. Mol. Phys., 48, 144027
Guerra, M., Amaro, P., Santos, J. P., & Indelicato, P. 2017, At. Data Nucl. Data Tables, 117, 439
Hollenbach, D., & McKee, C. F. 1989, ApJ, 342, 306
Indebetouw, R., & Shull, J. M. 2004, ApJ, 605, 205
Indelicato, P., & Desclaux, J. P. 1990, Phys. Rev. A, 42, 5139
Jakubowicz, H., & Moores, D. L. 1981, J. Phys. B At. Mol. Phys., 14, 3733
Kim, Y.-K., & Rudd, M. E. 1994, Phys. Rev. A, 50, 3954
Kim, Y.-K., Santos, J. P., & Parente, F. 2000, Phys. Rev. A, 62, 052710
Knopp, H., Teng, H., Ricz, S., Schippers, S., & Müller, A. 2001, Phys. Scr. Vol. T, 92, 379
Larson, R. B. 1981, MNRAS, 194, 809
Lecointre, J., Kouzakov, K. A., Belic, D. S., et al. 2013, J. Phys. B At. Mol. Phys., 46, 205201
Lennon, M. A., Bell, K. L., Gilbody, H. B., et al. 1988, J. Phys. Chem. Ref. Data, 17, 1285
Llovet, X., Powell, C. J., Salvat, F., & Jablonski, A. 2014, J. Phys. Chem. Ref. Data, 43, 013102
Loch, S. D., Witthoeft, M., Pindzola, M. S., et al. 2005, Phys. Rev. A, 71, 012716
Lotz, W. 1967, ApJS, 14, 207
Lotz, W. 1968, Z. Phys., 216, 241
Ludlow, J. A., Loch, S. D., Pindzola, M. S., et al. 2008, Phys. Rev. A, 78, 052708
Masai, K. 1984, Ap&SS, 98, 367
Mattioli, M., Mazzitelli, G., Finkenthal, M., et al. 2007, J. Phys. B At. Mol. Phys., 40, 3569
Moores, D. L. 1972, J. Phys. B At. Mol. Phys., 5, 286
Mori, M., & Sugihara, M. 2001, J. Comput. Appl. Math., 127, 287
Pattard, T., & Rost, J. M. 1999, Phys. Scr. Vol. T, 80, 295
Pavlovski, G., Smith, M. D., Mac Low, M.-M., & Rosen, A. 2002, MNRAS, 337, 477
Pindzola, M. S., Ballance, C. P., & Loch, S. D. 2012, J. Phys. Conf. Ser., 388, 062016
Pradhan, A. K., & Nahar, S. N. 2011, Atomic Astrophysics and Spectroscopy (Cambridge: Cambridge University Press)
Reilman, R. F., & Manson, S. T. 1979, ApJS, 40, 815
Rodrigues, G. C., Indelicato, P., Santos, J. P., Patté, P., & Parente, F. 2004, At. Data Nucl. Data Tables, 86, 117
Schmutzler, T., & Tscharnuter, W. M. 1993, A&A, 273, 318
Shapiro, P. R., & Moore, R. T. 1976, ApJ, 207, 460
Slavin, J. D., Shull, J. M., & Begelman, M. C. 1993, ApJ, 407, 83
Suno, H., & Kato, T. 2006, At. Data Nucl. Data Tables, 92, 407
Sutherland, R. S., & Dopita, M. A. 1993, ApJS, 88, 253
Takahasi, H., & Mori, M. 1974, Publ. Res. Inst. Math. Sci., 9, 721
Wang, Y., Zatsarinny, O., & Bartschat, K. 2013, Phys. Rev. A, 87, 012704
Wolfire, M. G., Hollenbach, D., McKee, C. F., Tielens, A. G. G. M., & Bakes, E. L. O. 1995, ApJ, 443, 152
Wolfire, M. G., McKee, C. F., Hollenbach, D., & Tielens, A. G. G. M. 2003, ApJ, 587, 278
Woodruff, P. R., Hublet, M.-C., Harrison, M. F. A., & Brook, E. 1978, J. Phys. B At. Mol. Phys., 11, L679
Yamada, I., Danjo, A., Hirayama, T., et al. 1989, J. Phys. Soc. Jpn., 58, 1585
Younger, S. M. 1980, Phys. Rev. A, 22, 111
Younger, S. M. 1981, J. Quant. Spectrosc. Radiat. Transf., 26, 329